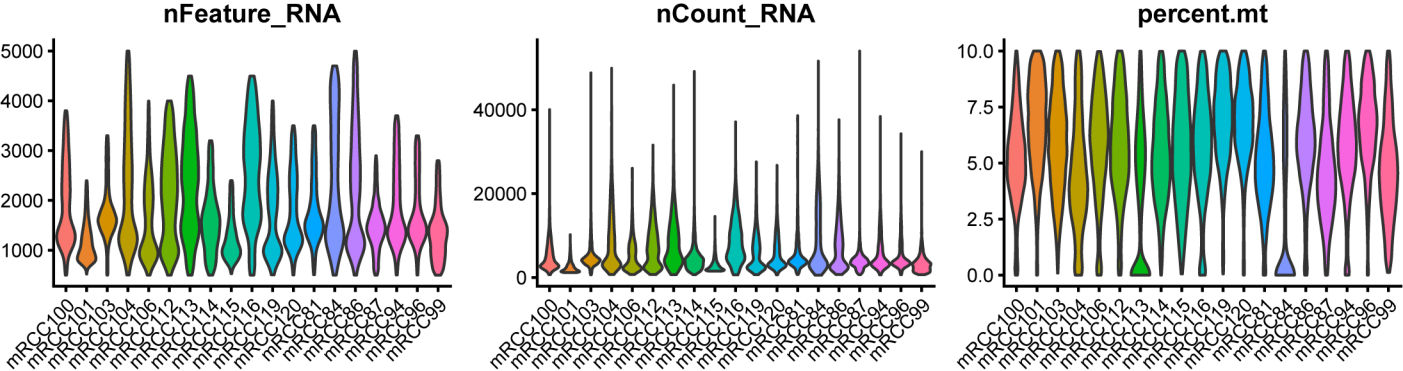

Figure S1 Quality control (QC) of scRNA-seq data. (nFeature, number of genes; nCount, unique molecular identifiers; percent.mt, percentage of mitochondrial genes).

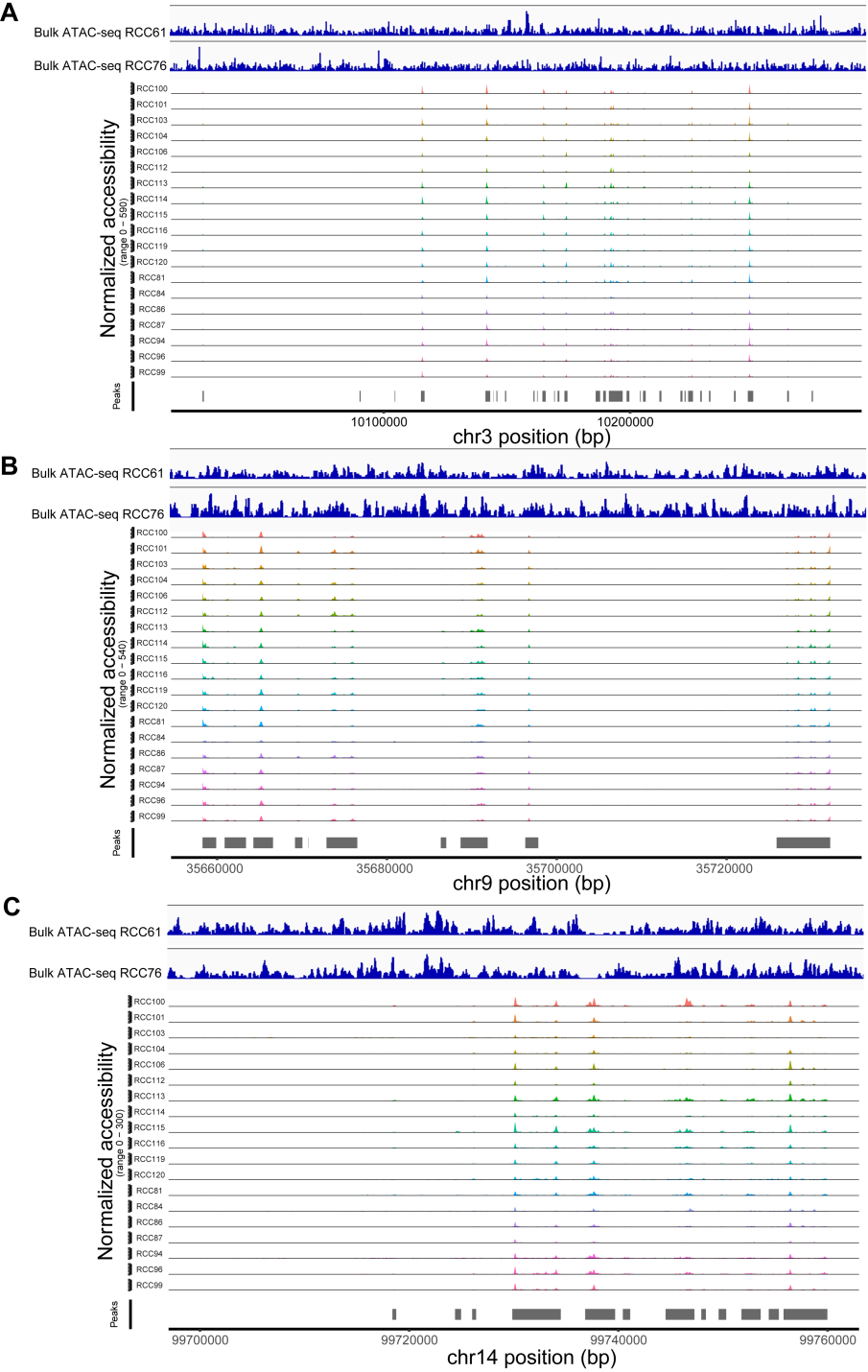

Figure S2 Comparison of scATAC-seq with bulk ATAC-seq in human ccRCC. Chromatin accessibility regions of scATAC-seq and bulk ATAC-seq on chromosome 3 (A), chromosome 9 (B) and chromosome 14 (C) were compared. The scATAC-seq were obtained from 19 samples, whereas bulk ATAC-seq from two samples.

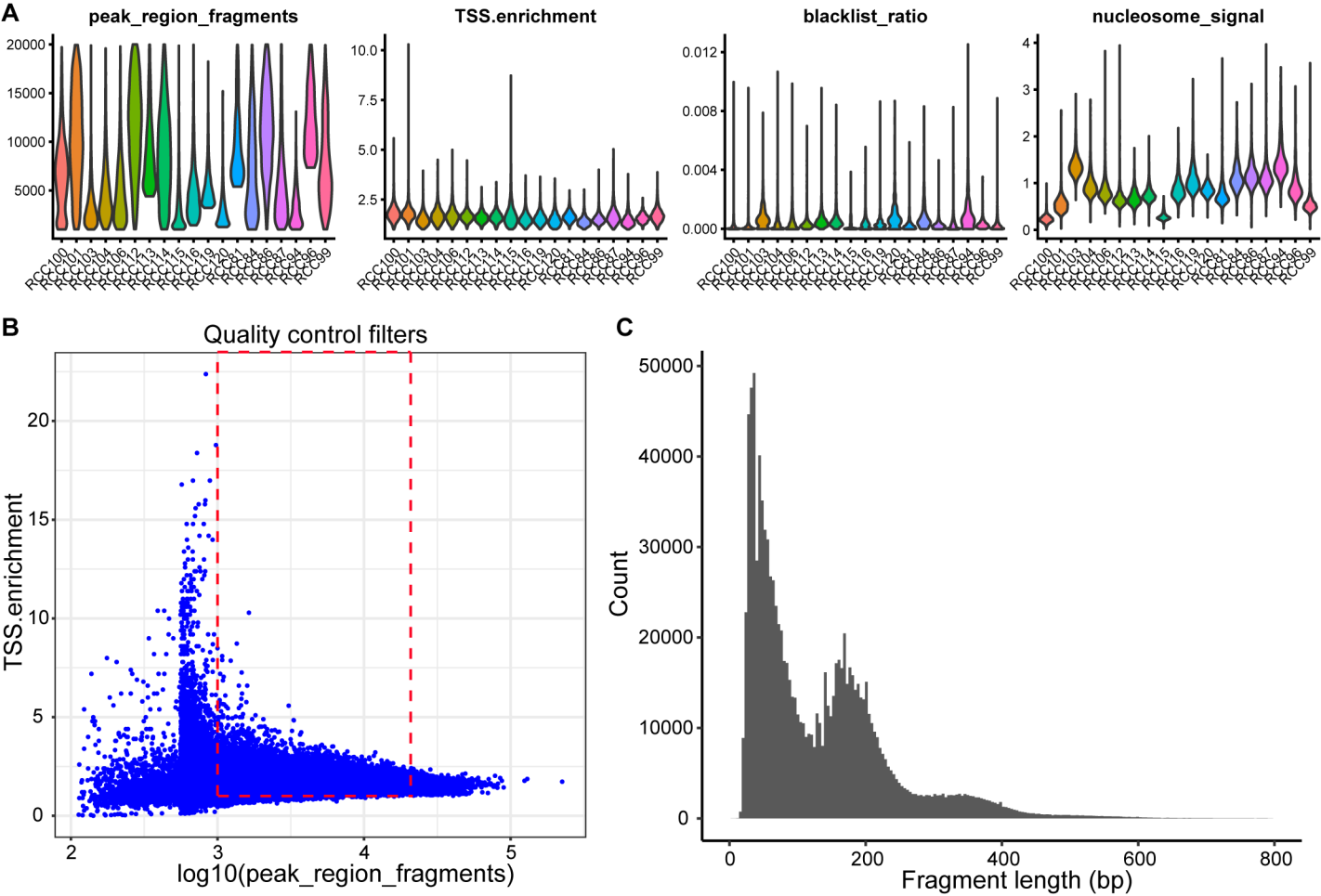

Figure S3 Quality control (QC) of scATAC-seq data. (A) QC of scATAC-seq data. (B) High-quality cells were selected according to TSS and peaks. (C) Fragment length was detected by scATAC-seq. (TSS, transcription start site).

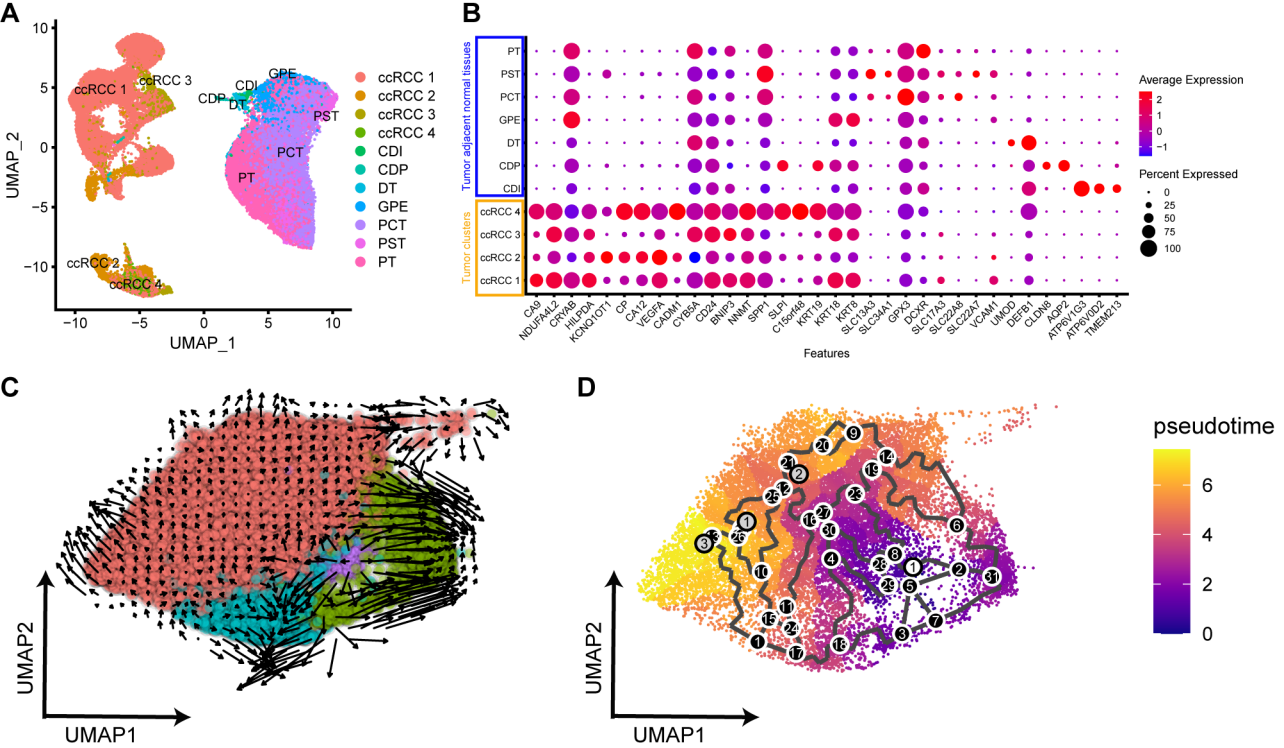

Figure S4 scRNA-seq revealed the biological characteristics of tumor cells. (A) UMAP projection of tumour cells and tumor adjacent normal epithelial cells. Normal epithelial cells were proximal tubular cells (PT), proximal straight tubule cells (PST), proximal convoluted tubule cells (PCT), glomerular parietal epithelial cells (GPE), distal tubule cells (DT), collecting duct principal cells (CDP) and collecting duct intercalated cells (CDI). (B) Bubble plot showed the differences of gene expression between tumor adjacent normal cells and tumor cells. (C) Pseudotime analysis of ccRCC cells by using RNA velocity to reconstruct the developmental lineages (arrows represent direction, and lengths represent rate). (D) Monocle3 analysis on the subset of ccRCC clusters resulted in trajectory.

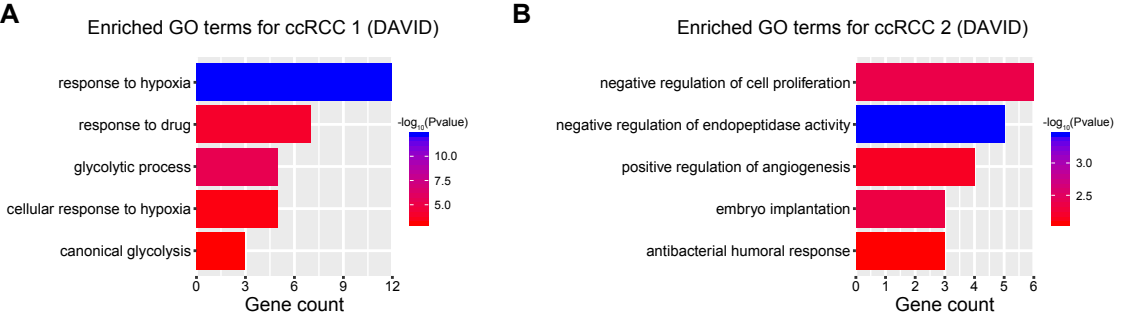

Figure S5 GO enrichment analysis revealed the biological characteristics of tumor cells. (A–D) GO enrichment analysis of each tumour cell type for biological process.

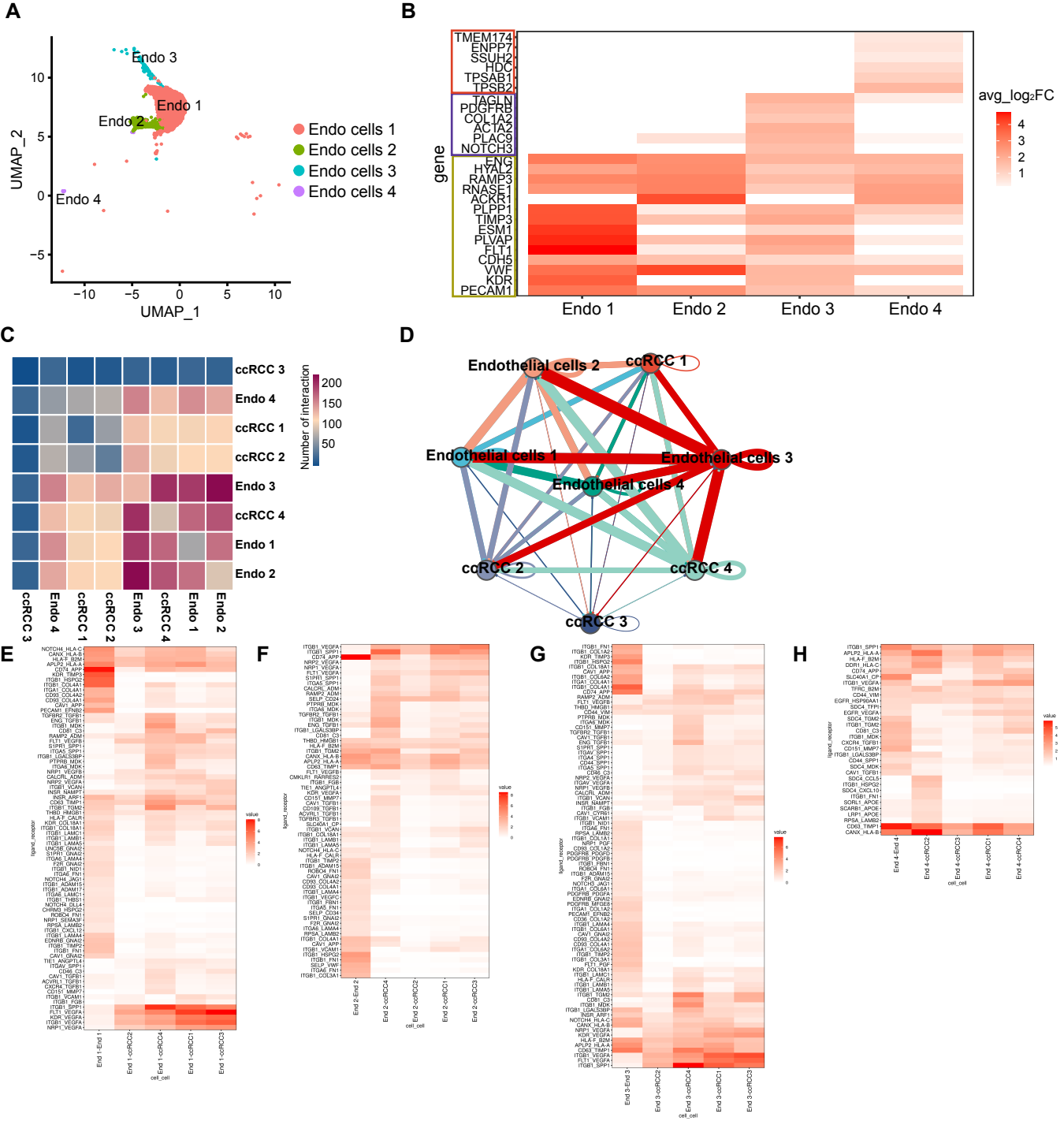

Figure S6 Single-cell transcriptome characterisation of endothelial cells and drug sensitivity of endothelial and tumour cells. (A) UMAP plot of four endothelial cell types. (B) Comparison of the DEGs in different endothelial cell types (Endo 1, Endo 2, Endo 3 and Endo 4). (C) Heat map of the number of receptor/ligands interacting with endothelial and tumour cells. (D)Potential specific interactions between endothelial cells and tumour cells. The nodes represent the cell population, and the line thickness represents the number of important ligand–receptor pairs. (E-H) The key L/R receptor pairs between endothelial and tumor cells.

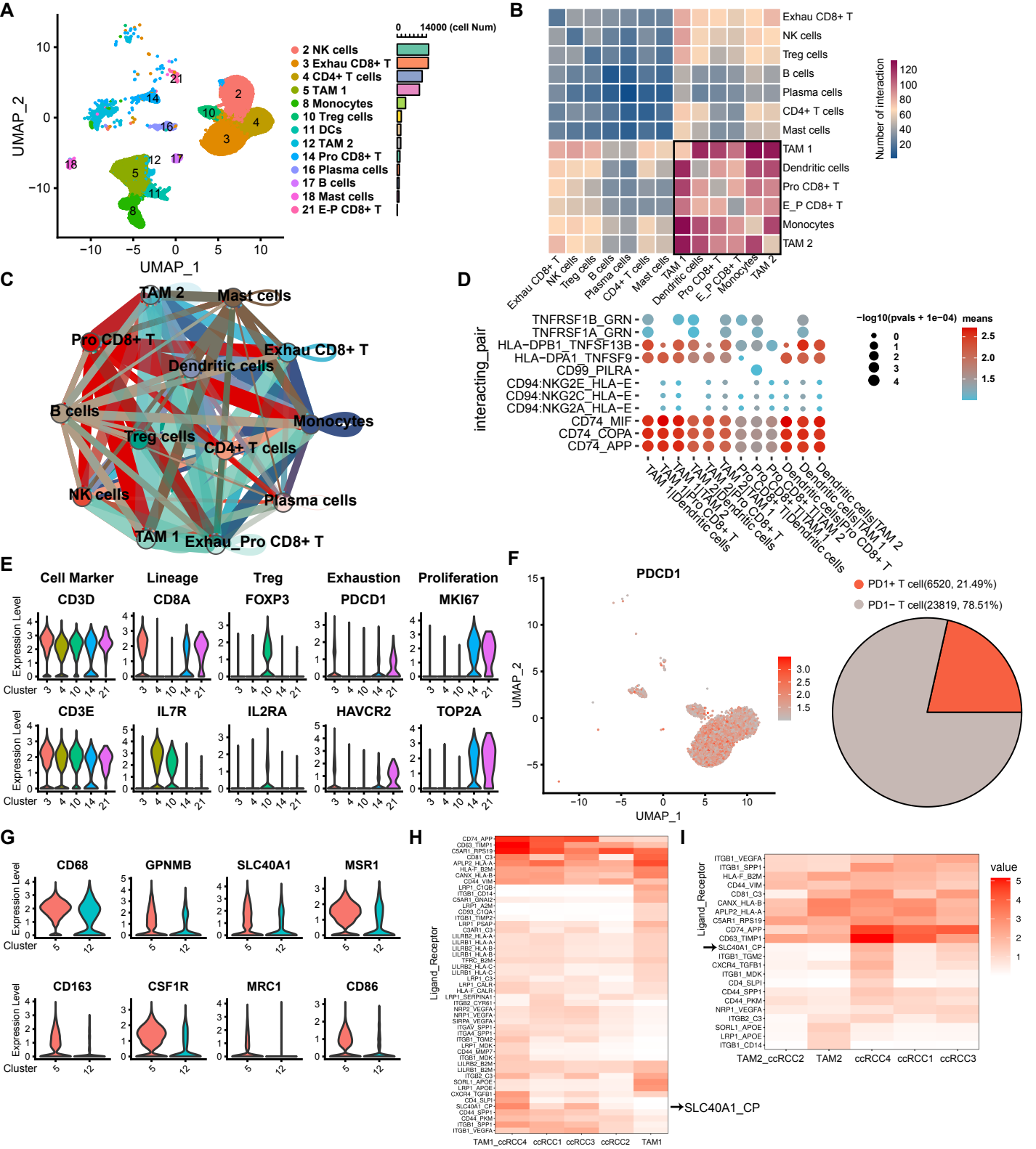

Figure S7 Single-cell transcriptome characterisation of immune cells in ccRCC. (A) UMAP plot of different immune cell types. (B) Heat map of the number of receptor/ligands interacting with immune cell types. (C) Interaction network constructed by CellPhoneDB. Each line colour indicated the ligands expressed by the cell population represents by the same colour (labelled), and the line thickness is proportional to the number of ligands. (D) Overview of selected ligand–receptor interactions of cells in immune cell types. (E) Violin plots showing cell markers expressed in cluster 3 (Exhau CD8+ T cells), 4 (CD4+ T cells), 10 (Treg cells), 14 (Pro CD8+ T cells) and 21 (E-P CD8+ T cells). (F) UMAP plot of PDCD1 positive and negative T cells; Pie chart showing the cell proportion of T cell. (G) Violin plots showing cell markers expressed in TAM1 and TAM2. (H, I) Ligand–receptor interactions between ccRCC and TAM.

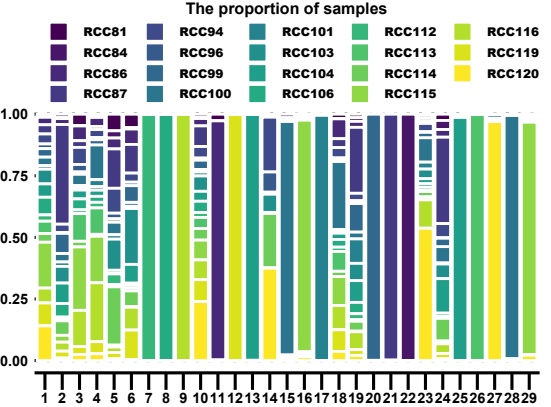

Cell types

1 NKT cells (9,436)
2 CD4+ T cells (5,874)
3 Endo cells 1 (5,185)
4 CAF 1 (4,386)
5 NK 1 (3,215)
6 NK 2 (2,990)
7 ccRCC 1 (2,778, RCC112 mainly)
8 ccRCC 2 (2,433, RCC106 mainly)
9 ccRCC 3 (2,176, RCC116 mainly)
10 B cells (2,105)
11 ccRCC 4 (2,078, RCC86 mainly)
12 ccRCC 5 (1,999, RCC119 mainly)
13 ccRCC 6 (1,832, RCC104 mainly)
14 ccRCC 7 (1,573, RCC120 mainly)
15 Endo cells 2 (1,505)
16 *CDC37+* cells (1,445)
17 ccRCC 8 (1,293, RCC101 mainly)
18 Endo cells 3 (1,217)
19 CD56+ NK (1,199)
20 ccRCC 9 (999, RCC99 mainly)
21 ccRCC 10 (838, RCC87 mainly)
22 ccRCC 11 (808, RCC84 mainly)
23 *SHCBP1+* cells (745)
24 CAF 2 (707)
25 ccRCC 12 (604, RCC104 mainly)
26 ccRCC 13 (587, RCC113 mainly)
27 ccRCC 14 (568, RCC120 mainly)
28 ccRCC 15 (560, RCC100 mainly)
29 ccRCC 16 (558, RCC115 mainly)

Figure S8 Proportion of 19 ccRCC samples in each cell type.

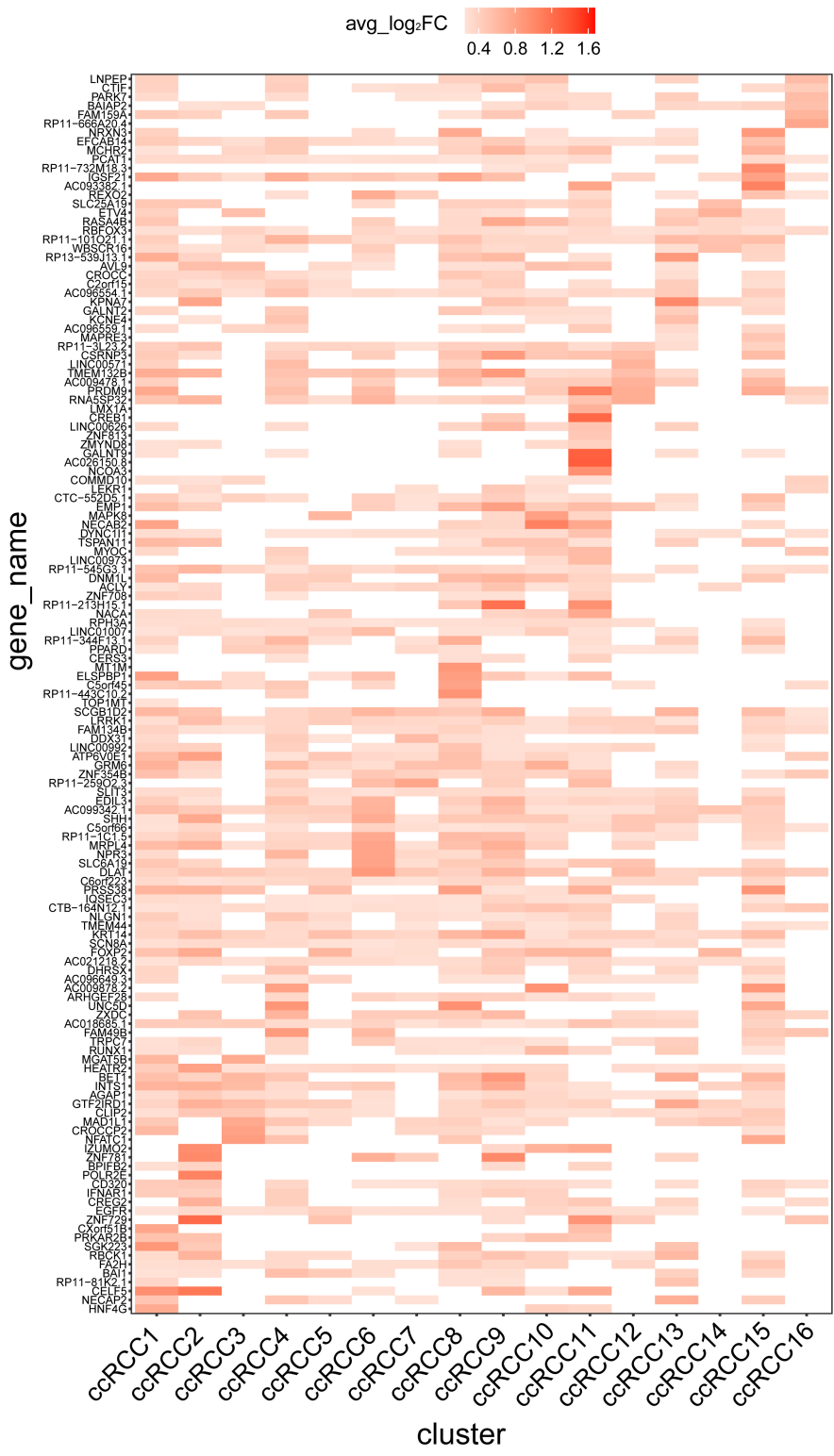

Figure S9 Heatmap representation of the scaled expression of the top 10 peaks that match to the gene region in each tumour cell subtype.

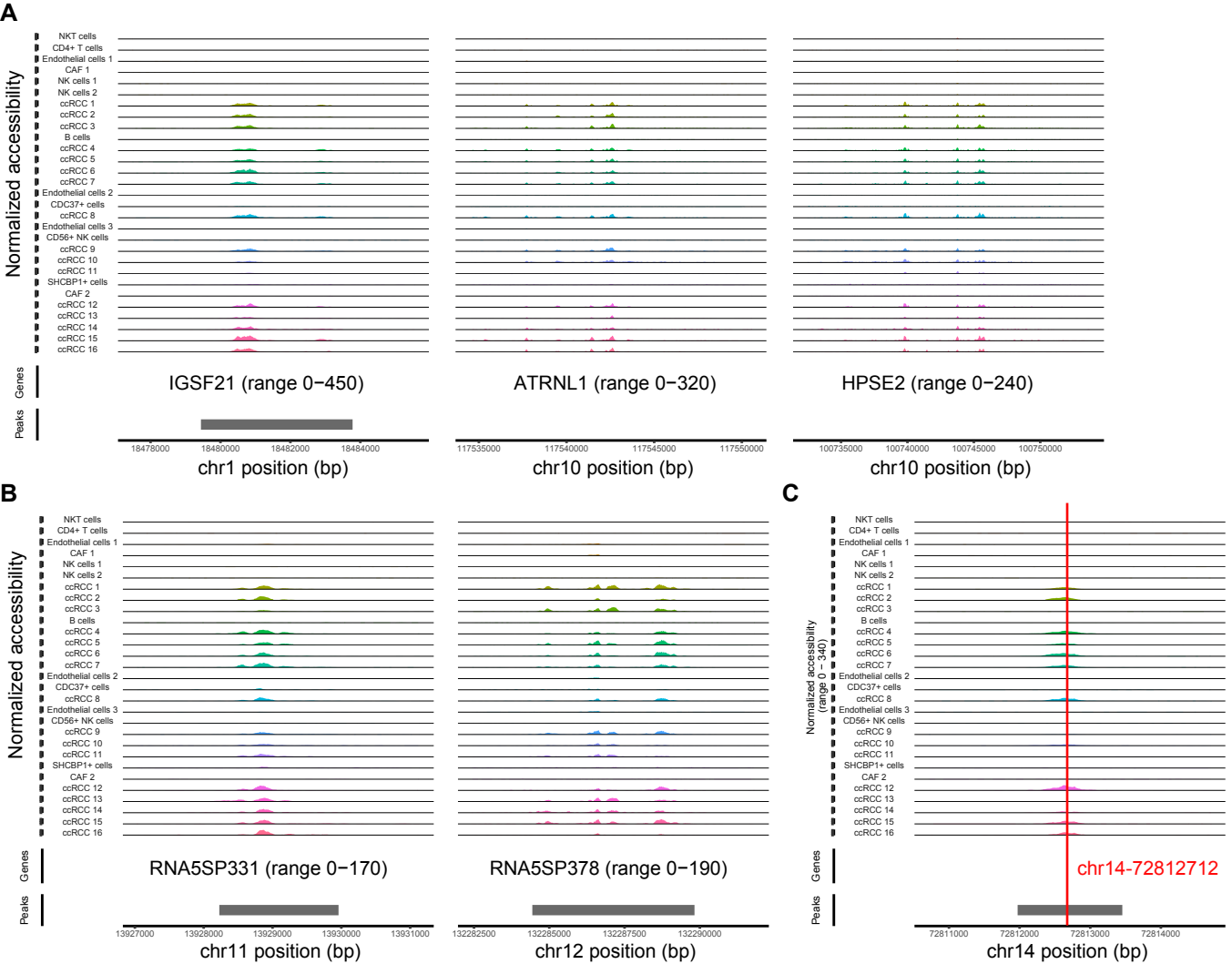

Figure S10 scATAC-seq reveals the regulatory characteristics of tumour cells in ccRCC. (A) Regulatory regions with tumour-cell-specific accessibility. (B) rRNA regions with tumour-cell-specific accessibility. (C) Chromatin region of susceptible locus identified by GWAS.

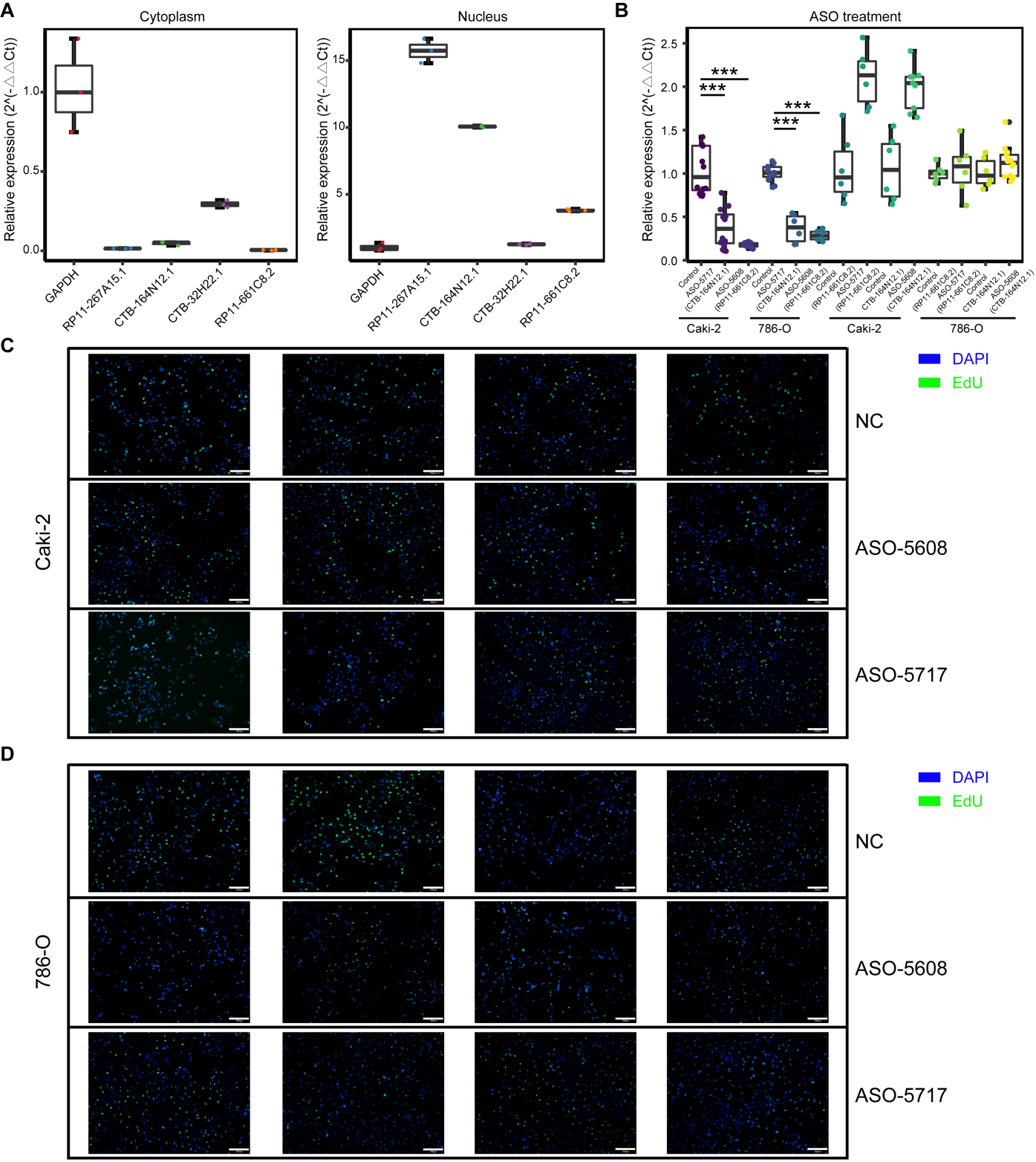

Figure S11 Biological functions of lncRNAs in vitro. (A) lncRNA expression levels in the cytoplasm or nucleus of RCC cell lines. GAPDH as control group. (B) lncRNA expression levels in RCC cell lines after 48 h ASO treatment (***: $p < 0.001$). ASO-5717 hit the CTB-164N12.1 specifically, while ASO-5608 hit the RP11-661C8.2. (C, D) EdU proliferation assay was performed 48 h after the transfection of Caki-2 and 786-O cells with a negative control, ASO-5717 and AS0-5608.

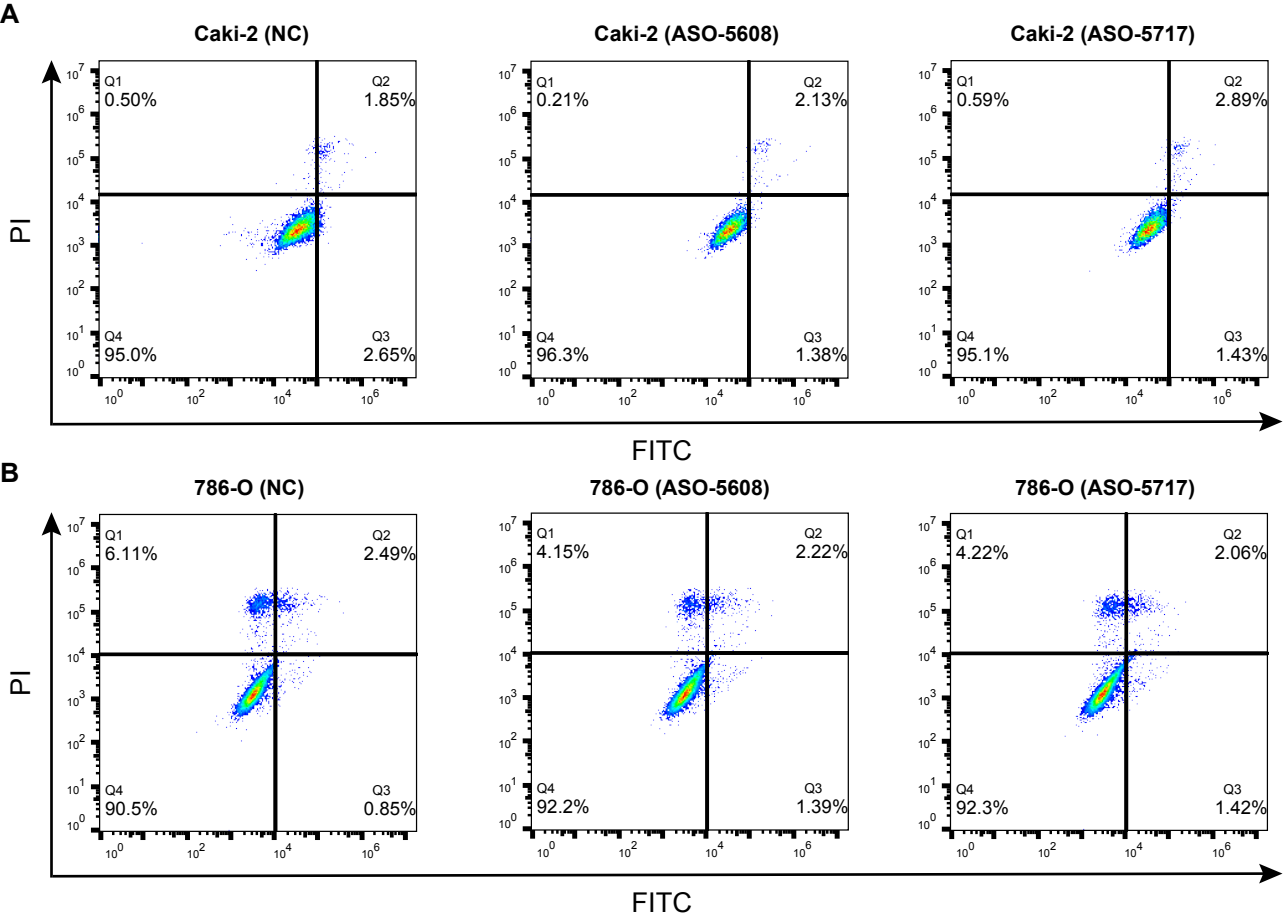

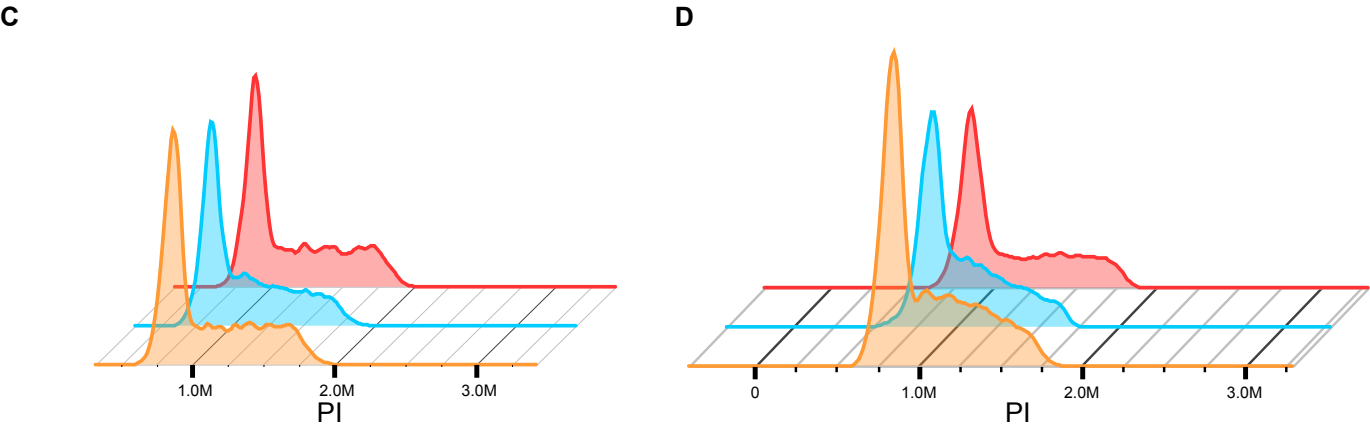

	Sample Name	G1 (%)	G2 (%)
	Caki-2 ASO5717	49.7	19.8
	Caki-2 ASO5608	55.4	19.4
	Caki-2 NC	51.0	23.1

	Sample Name	G1 (%)	G2 (%)
	786-O ASO5717	45.9	8.67
	786-O ASO5608	44.6	0.82
	786-O NC	43.6	2.97

Figure S12 Cell apoptosis and cell cycle functions of lncRNAs in ccRCC cell lines. (A, B) Apoptosis assay in Caki-2 cells (A) and 786-O cells (B) using flow cytometry after staining with annexin V-FITC/PI. (C, D) Cell cycle analysis in Caki-2 cells (C) and 786-O cells (D) using flow cytometry after staining with propidium iodide (PI). ASO-5717 hit the *CTB-164N12.1* specifically, while ASO-5608 hit the *RP11-661C8.2*.

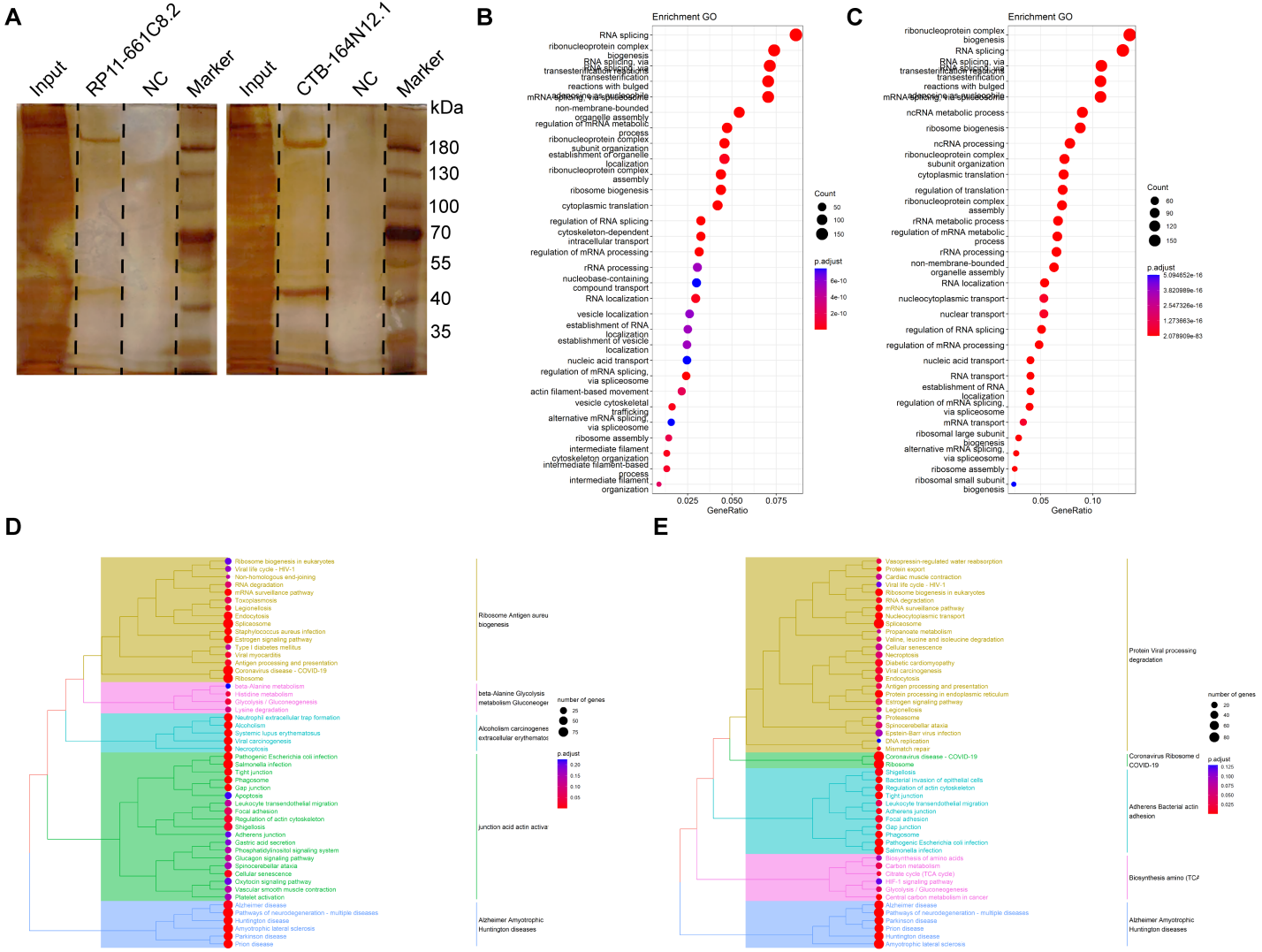

Figure S13 Results of RNA pulldown and protein mass spectrometry. (A) The proteins of *RP11-661C8.2* and *CTB-164N12.1* were verified by silver staining. GO analysis results of proteins bound to *RP11-661C8.2* (B) and *CTB-164N12.1* (C). KEGG analysis results of proteins bound to *RP11-661C8.2* (D) and *CTB-164N12.1* (E).

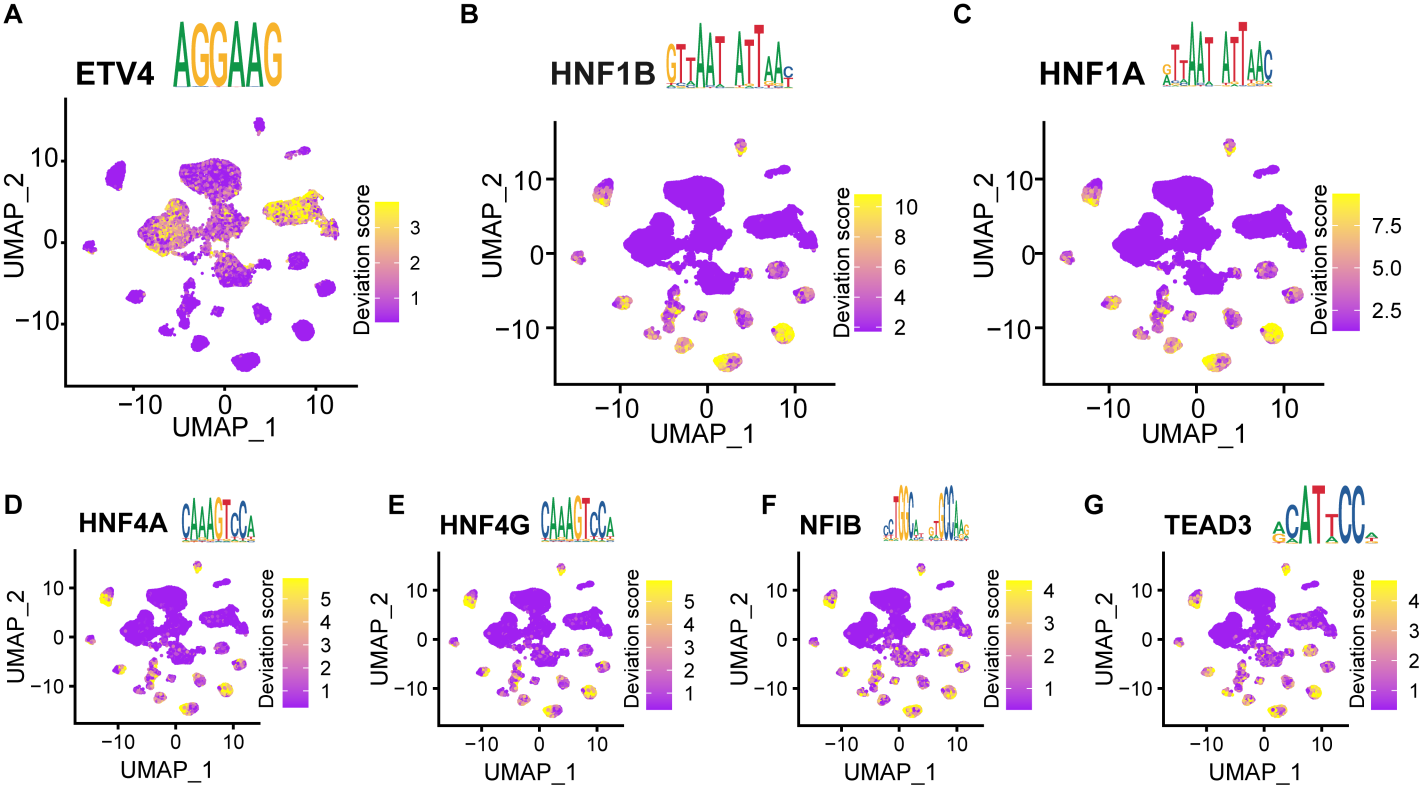

Figure S14 UMAP plot shows that cell-type-specific TFs and their motifs were identified by scATAC-seq. UMAP projection of these TFs and motifs, such as ETV4 (A), HNF1B (B), HNF1A (C), HNF4A (D), HNF4G (E), NFIB (F) and TEAD3 (G).

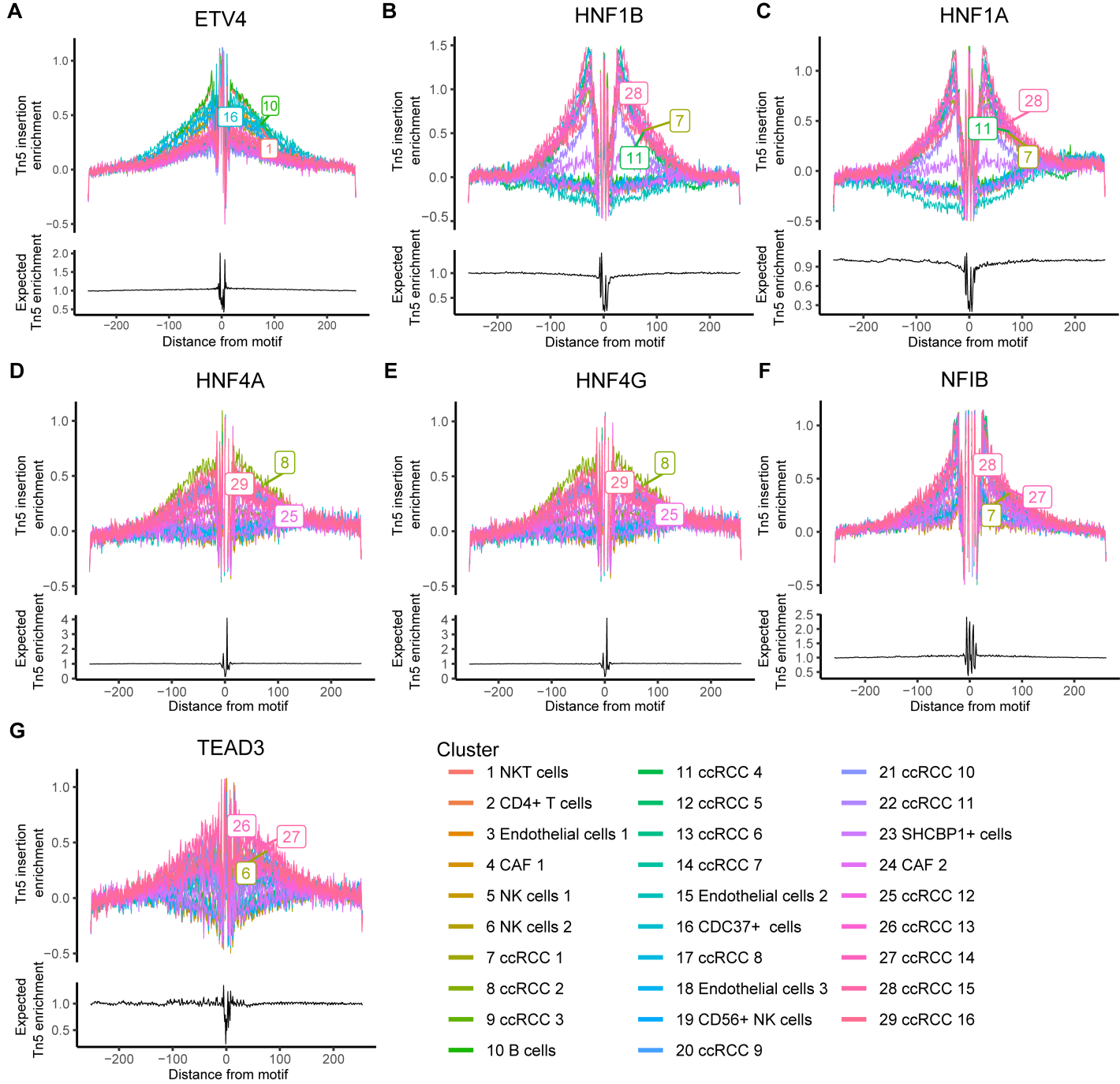

Figure S15 TF footprints of ETV4 (A), HNF1B (B), HNF1A (C), HNF4A (D), HNF4G (E), NFIB (F) and TEAD3 (G) were identified by scATAC-seq. The Tn5 insertion bias track is shown below.

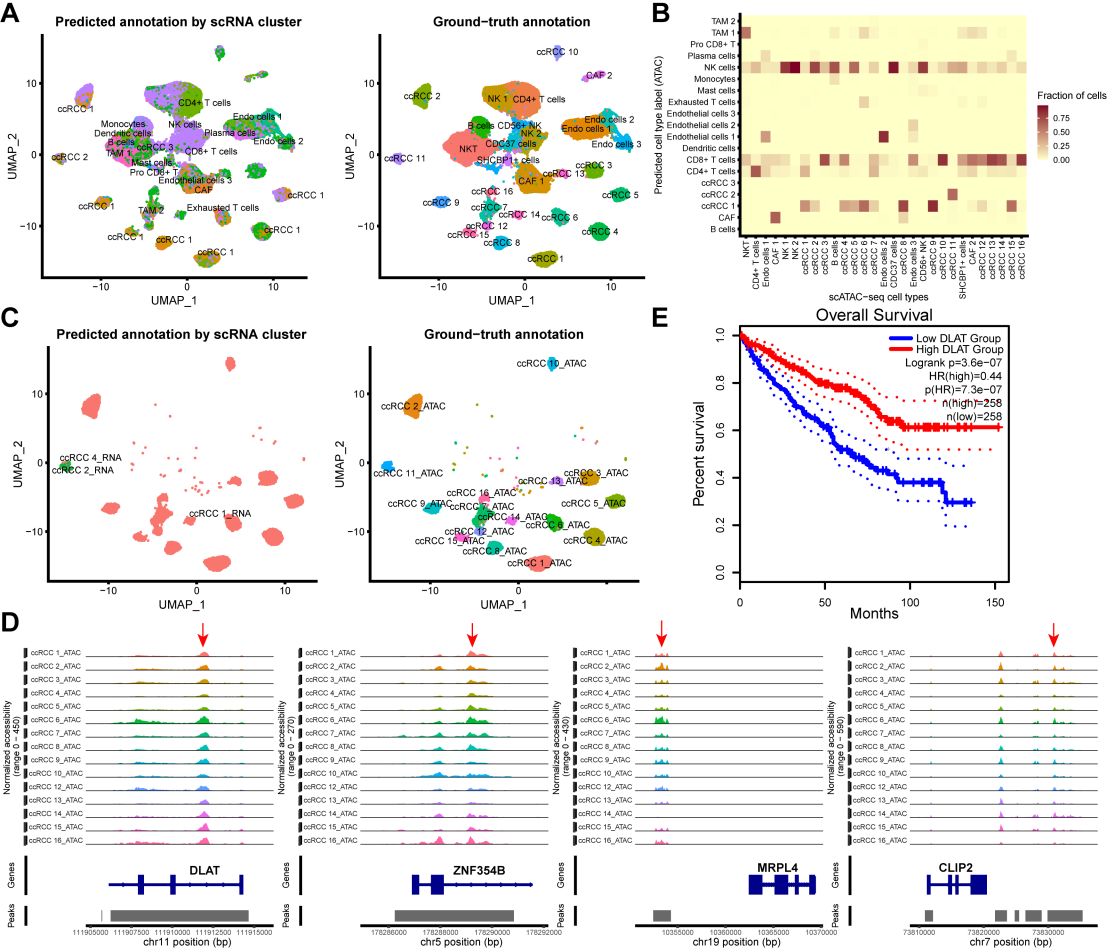

Figure S16 The cell types from scATAC-seq were predicted by scRNA-seq results. (A) All cell types from scATAC-seq were predicted by scRNA-seq results. (B) Heatmap showing the proportions of all cells from each scATAC-seq cluster (x axis) that were annotated with cluster labels transferred from scRNA-seq clusters (y axis). (C) Tumour cell types from scATAC-seq were predicted by scRNA-seq results. (D) Common chromatin accessibility regions of 15 tumor cell subtypes from scATAC-seq (red arrows). (E) Overall survival for the TCGA ccRCC cohorts based on high DLAT signature (median) versus low signature expression. Log-rank test was used to compare the survival between the two groups. P = 3.6e-7.